Journal of Physics: Conference Series **299** (2011) 012005 doi:10.1088/1742-6596/299/1/012005

Spin Structure Functions

J. P. Chen[1], A. Deur[1], S. Kuhn[2] and Z. E. Meziani[3]

[1] Jefferson Lab, Newport News, Virginia 23606, USA
[2] Old Dominion University, Norfolk, Virginia 23529, USA
[3] Temple University, Philadelphia, Pennsylvania 19122, USA

Abstract. Spin-dependent observables have been a powerful tool to probe the internal structure of the nucleon and to understand the dynamics of the strong interaction. Experiments involving spin degrees of freedom have often brought out surprises and puzzles. The so-called "spin crisis" in the 1980s revealed the limitation of naive quark-parton models and led to intensive worldwide efforts, both experimental and theoretical, to understand the nucleon spin structure. With high intensity and high polarization of both the electron beam and targets, Jefferson Lab has the world's highest polarized luminosity and the best figure-of-merit for precision spin structure measurements. It has made a strong impact in this subfield of research. This chapter will highlight Jefferson Lab's unique contributions in the measurements of valence quark spin distributions, in the moments of spin structure functions at low to intermediate Q^2, and in the transverse spin structure.

1. Introduction

1.1. The spin structure functions g_1 and g_2

For inclusive polarized electron scattering off a polarized nucleon target, the cross section depends on four structure functions, $F_1(x,Q^2)$, $F_2(x,Q^2)$, $g_1(x,Q^2)$ and $g_2(x,Q^2)$, where F_1 and F_2 are the unpolarized structure functions and g_1 and g_2 the polarized ones. In the naive quark parton model, F_1 or F_2 gives the quark momentum distribution and g_1 probes the quark spin distribution [1]:

$$g_1^p = \frac{1}{2}\left(\frac{4}{9}(\Delta u + \Delta\overline{u}) + \frac{1}{9}(\Delta d + \Delta\overline{d}) + \frac{1}{9}(\Delta s + \Delta\overline{s})\right), \quad (1)$$

where Δu ($\Delta\overline{u}$), Δd ($\Delta\overline{d}$), and Δs ($\Delta\overline{s}$), are the polarized $u(\overline{u})$, $d(\overline{d})$, and $s(\overline{s})$ quark (antiquark) distributions (number of quarks with their helicity aligned minus those with their helicity anti-aligned with the nucleon spin), respectively, and heavy quark (c, b and t) contributions are neglected. In naive quark models, it is often assumed that the three flavors of quarks follow the SU(3) flavor symmetry. Then the knowledge from the β decays of the neutron and the hyperons can be combined with the first moment (Γ_1) of g_1 to determine the spin-flavor decomposition. The β-decay constants determine the octet parts of the flavor contributions and, together with Γ_1, can be used to reveal the value of the flavor singlet contribution, the total quark contribution to the proton spin. Consequently, precise measurements of g_1 have been a main goal of the nucleon spin structure study. In the QCD-improved parton model, the simple interpretation of g_1 as the quark spin distribution holds only at leading twist. Gluon radiations come in at higher orders leading to logarithmic scaling violation, which are well described by the QCD evolution

equations. Higher twist effects ($1/Q^{t-2}$ power corrections, where t is the twist rank) can become important in the low Q^2 region.

The second spin structure function, g_2, is related to the transverse spin structure, $g_T = g_1 + g_2$. Although g_2 has no simple interpretation in the naive parton model, it provides clean information on the quark-gluon correlations through higher twist effects. The standard operator product expansion (OPE) analysis has shown that at large Q^2, g_2 is related to matrix elements of both twist-2 and twist-3 operators. Neglecting quark masses, g_2 can be separated into a twist-2 (Wandzura-Wilczek) and a twist-3 (and higher) term:

$$g_2(x, Q^2) = g_2^{WW}(x, Q^2) + \overline{g_2}(x, Q^2), \tag{2}$$

where the twist-3 (and higher) term, $\overline{g_2}$, is not $1/Q$ suppressed with respect to the twist-2 term. The twist-2 term can be determined from the twist-2 part of g_1 as [2]

$$g_2^{WW}(x, Q^2) = -g_1(x, Q^2) + \int_x^1 \frac{g_1(y, Q^2)}{y} dy. \tag{3}$$

Therefore, g_2 provides a clean way to study twist-3 effects. In addition, at high Q^2, the x^2-weighted moment, d_2, is a twist-3 matrix element and is related to the color polarizabilities [3]:

$$d_2(Q^2) = \int_0^1 x^2 \left(g_2(x, Q^2) - g_2^{WW}(x, Q^2) \right) dx. \tag{4}$$

Predictions for d_2 exist from lattice QCD [4] and various models [5, 6, 7].

1.2. Virtual photon asymmetries

Other physics observables of interest are the virtual photon-nucleon asymmetries A_1 and A_2:

$$A_1 = \frac{g_1 - (Q^2/\nu^2) g_2}{F_1} \approx \frac{g_1}{F_1}, \tag{5}$$

$$A_2 = \frac{Q^2}{\nu^2} \frac{g_1 + g_2}{F_1}. \tag{6}$$

The high-x region is of special interest for A_1 measurements because there the valence quark contributions are expected to dominate. With sea quark and explicit gluon contributions expected to be unimportant, it is a clean region to test our understanding of nucleon structure. Relativistic constituent quark models [8] should be applicable in this region and perturbative QCD (pQCD) [9] can be used to make predictions in the large-x limit. To first approximation, the constituent quarks in the nucleon are described by SU(6) wave functions. SU(6) symmetry leads to the following predictions [10]:

$$A_1^p = 5/9; \quad A_1^n = 0; \quad \Delta u/u = 2/3; \quad \Delta d/d = -1/3. \tag{7}$$

Relativistic constituent quark models (RCQM) with broken SU(6) symmetry, *e.g.*, the hyperfine interaction model [8], predict that as $x \to 1$:

$$A_1^p \to 1; \quad A_1^n \to 1; \quad \Delta u/u \to 1; \quad \text{and} \quad \Delta d/d \to -1/3. \tag{8}$$

In the RCQM, relativistic effects lead to a nonzero orbital angular momentum and reduce the valence quark contributions to the nucleon spin from 1 to 0.6–0.75.

Another approach is leading order pQCD [9], which assumes the quark orbital angular momentum to be negligible and leads to hadron helicity conservation. It yields:

$$A_1^p \to 1; \quad A_1^n \to 1; \quad \Delta u/u \to 1; \quad \text{and} \quad \Delta d/d \to 1. \tag{9}$$

Not only are the limiting values of A_1 and polarized PDFs as $x \to 1$ important, but also their behavior in the high-x region, which is sensitive to the dynamics in the valence quark region. An improved approach [11] in pQCD, including quark orbital angular momentum (and therefore not requiring hadron helicity conservation), shows a different behavior at large x while keeping the same limiting value at $x = 1$. In particular, the approach of $\Delta d/d$ towards unity only sets in at a significantly larger x than predicted by hadron helicity conservation.

1.3. Sum rules

Sum rules involving the spin-structure functions offer an important opportunity to study QCD. Spin sum rules relate the moments of the spin-structure functions to the nucleon's static properties (as in the Bjorken or Gerasimov, Drell and Hearn (GDH) sum rules), or real or virtual Compton amplitudes, which can be calculated theoretically (as in the generalized GDH or the forward spin polarizability sum rules). Refs. [12, 13] provide comprehensive reviews on this subject. The Ellis-Jaffe sum rule [14] was the first to be experimentally studied. By assuming SU(3) flavor symmetry and that the strange sea quarks are unpolarized, this sum rule links, in the Bjorken limit ($Q^2 \to \infty$), the first moment of g_1 to the polarized quark distributions Δu and Δd:

$$\Gamma_1^p \equiv \int_0^1 g_1^p dx \to \frac{1}{2}\left(\frac{4}{9}\Delta u + \frac{1}{9}\Delta d\right), \tag{10}$$

$$\Gamma_1^n \equiv \int_0^1 g_1^n dx \to \frac{1}{2}\left(\frac{4}{9}\Delta d + \frac{1}{9}\Delta u\right), \tag{11}$$

with the values given by the β-decay constants of the neutron and the hyperons. This sum rule has been experimentally found to be violated, resulting in the so-called "spin crisis" of the 1980s and the realization that at least some of the assumptions leading to Eqs. (10)–(11) are incorrect.

A sum rule on the first moment of g_2 also exists: the Burkhardt-Cottingham (BC)sum rule [15] states that the first moment of g_2 is zero at any Q^2:

$$\Gamma_2 \equiv \int_0^1 g_2(x, Q^2) dx = 0. \tag{12}$$

The sum rule assumes that g_2 has good convergence properties and is analytic in the $x \to 0$ limit. In recent years the Bjorken sum rule [16] at large Q^2 and the GDH sum rule [17] at $Q^2 = 0$ have attracted considerable experimental and theoretical efforts.

The Bjorken sum rule links the isovector part of the g_1 moment to g_A, the nucleon axial charge that governs neutron β-decay. It has been extended to finite Q^2 with the OPE technique:

$$\Gamma_1^{p-n}(Q^2) \equiv \int_0^1 (g_1^p - g_1^n) dx = \frac{g_A}{6}\left(1 - \frac{\alpha_s}{\pi} - 3.58\left(\frac{\alpha_s}{\pi}\right)^2 - 20.21\left(\frac{\alpha_s}{\pi}\right)^3 + \cdots\right) + \mathcal{O}\left(\frac{1}{Q^2}\right). \tag{13}$$

It is a rigorous sum rule based on general principles. Studies of Γ_1^N and of the Bjorken sum rule at high Q^2 can be used to extract higher twist information, such as the OPE matrix element f_2. These moments are also well suited for lattice QCD calculations.

The GDH sum rule applies to the opposite end of the Q^2 scale and links the transverse-transverse interference cross section for photoproduction σ_{TT} to the nucleon anomalous moment κ:

$$\int_{\nu_0}^{\infty} \frac{\sigma_{TT}(\nu)}{\nu} d\nu = -\frac{2\pi^2 \alpha \kappa^2}{M^2}. \tag{14}$$

It is, too, a rigorous sum rule. For electroproduction, σ_{TT} can be expressed in term of g_1 and g_2. This allows one to generalize the GDH sum rule [18] to nonzero Q^2 and connect it with the Bjorken sum rule. It provides a clean way to test theories with experimental data over the entire Q^2 range.

The generalized spin polarizabilities γ_0 and δ_{LT} are higher moments of σ_{TT} and σ_{LT} (the longitudinal-transverse interference cross section) and are derived in a similar manner to the generalized GDH sum rule.

$$\gamma_0(Q^2) = \left(\frac{1}{2\pi^2}\right) \int_{\nu_0}^{\infty} \frac{K(\nu, Q^2)}{\nu} \frac{\sigma_{TT}(\nu, Q^2)}{\nu^3} d\nu, \tag{15}$$

$$\delta_{LT}(Q^2) = \left(\frac{1}{2\pi^2}\right) \int_{\nu_0}^{\infty} \frac{K(\nu, Q^2)}{\nu} \frac{\sigma_{LT}(\nu, Q^2)}{Q\nu^2} d\nu, \tag{16}$$

where K is the virtual photon flux. They provide benchmark tests of chiral perturbation theory (χPT) calculations at low Q^2. Since the generalized polarizabilities have an extra $1/\nu^2$ weighting compared to the first moments (GDH sum or Γ_1), these integrals have smaller contributions from the large-ν region and converge much faster, which minimizes the uncertainty due to the experimentally inaccessible region at large ν. At low Q^2, the generalized polarizabilities have been evaluated with next-to-leading (NLO) order χPT calculations [19, 20]. One issue in the χPT calculations is how to properly include the nucleon resonance contributions, especially the Δ resonance. As was pointed out in Refs. [19, 20] , while γ_0 is sensitive to resonances, δ_{LT} is insensitive to the Δ resonance, making it an ideal candidate to test χPT calculations. Measurements of the generalized spin polarizabilities are an important step in understanding the dynamics of QCD in the chiral perturbation region.

1.4. Quark-hadron duality

In 1970, Bloom and Gilman [21] noted that the unpolarized nucleon resonance data averaged to the DIS scaling curve. This phenomenon, called quark-hadron duality, implies that there exists a domain where the fundamental (partonic) and effective (hadronic) descriptions of the strong force are both valid. In an earlier study [22] it was linked to the smallness of higher twists. It is natural to ask whether duality also holds for g_1 which, contrary to F_2 or F_1, can take negative values as well. The investigation of quark-hadron duality will aid in the study of the higher twist effects and the understanding of the high-x behavior in DIS. A detailed review can be found in [23].

1.5. Transversity

The transversity distributions, $\delta q(x, Q^2)$, are fundamental leading twist (twist-2) quark distributions, similar to the unpolarized and polarized parton distributions, $q(x, Q^2)$ and $\Delta q(x, Q^2)$. In quark-parton models, they describe the net transverse polarization of quarks in a transversely polarized nucleon. Several special features of the transversity distributions make them uniquely interesting:

- The difference between the transversity and the longitudinal distributions is purely due to relativistic effects. In the absence of relativistic effects (as in the nonrelativistic quark model, where boosts and rotations commute), the transversity distributions are identical to the longitudinally polarized distributions.
- The quark transversity distributions do not mix with gluonic effects [24] and therefore follow a much simpler evolution and have a valence-like behavior.
- The positivity of helicity amplitudes leads to the Soffer's inequality for the transversity[25]: $|\delta q| \leq \frac{1}{2}(q + \Delta q)$.
- The lowest moment of δq measures a simple local operator analogous to the axial charge, known as the "tensor charge", which can be calculated from lattice QCD.

Due to the chiral-odd nature of the transversity distribution, it cannot be measured in inclusive DIS experiments. In order to measure $\delta q(x, Q^2)$, an additional chiral-odd object is required, such as double-spin asymmetries in Drell-Yan processes, single target-spin azimuthal asymmetries in semi-inclusive DIS (SIDIS) reactions, double-spin asymmetries in Λ production from ep and pp reactions, and single-spin asymmetries in double pion production from ep scattering. The first results, from measurements performed by the HERMES [26] and COMPASS [27] collaborations with SIDIS, offered a first glimpse of possible effects caused by the transversity distributions.

2. Status of spin structure study prior to Jefferson Lab

The doubly polarized inclusive experiments in the DIS domain performed at CERN, SLAC and DESY are the cornerstones of our understanding of the nucleon spin structure. Their precise measurement of g_1 and A_1 (and g_2 and A_2 with less precision) taught us that:

• The strong force, responsible for the nucleon structure, is well described by pQCD at large Q^2, even in the spin sector (where the explicit spin degrees of freedom are important).

• Modeling the nucleon as a sum of quasi-free partons, corrected for QCD gluon radiation, is well suited to describe the longitudinal spin of the nucleon in the DIS domain. Thus, the nucleon spin S_N can be written as [30]:

$$S_N = \frac{1}{2} = \frac{1}{2}\Delta\Sigma + L_q + J_G, \tag{17}$$

where $\Delta\Sigma$ is the contribution of the quark spins to the nucleon spin, L_q is the quark orbital momentum contribution and J_G is the total gluon contribution.

• The quark spin contribution $\Delta\Sigma$ is about 0.3. Consequently, contributions from the gluon and/or the quark orbital momentum are significant [31].

• The Ellis-Jaffe sum rule (10)–(11), is violated for both nucleons. This implies that either the strange quarks are significantly polarized, or that the SU(3) symmetry is broken.

• The overall effects of higher twists are small for Q^2 greater than a few GeV^2.

In addition, the polarized distributions Δu_v, Δd_v, Δs and Δg were extracted through global analysis of inclusive DIS data (usually with certain assumptions), see Fig. 1 for a recent fit. The polarized gluon distribution has large uncertainties since it is accessible only indirectly by inclusive experiments. The Δs is negative, but also with large uncertainties.

From more recent semi-inclusive results we learned that:

• The polarized gluon distribution Δg at $x \simeq 0.1$ is compatible with zero. The various experimental results on $\Delta g/g$ are shown on Fig. 2. Since most of the gluon density lies at small x, this result hints that the integral of Δg, denoted by ΔG, is probably not as large as required by some explanations of the "spin crisis".

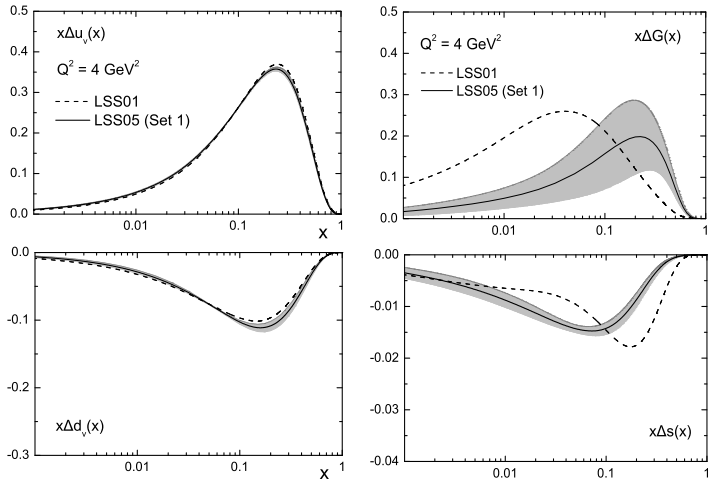

Figure 1. Polarized parton distributions in the proton by Leader, Stamenov and Sidorov [28].

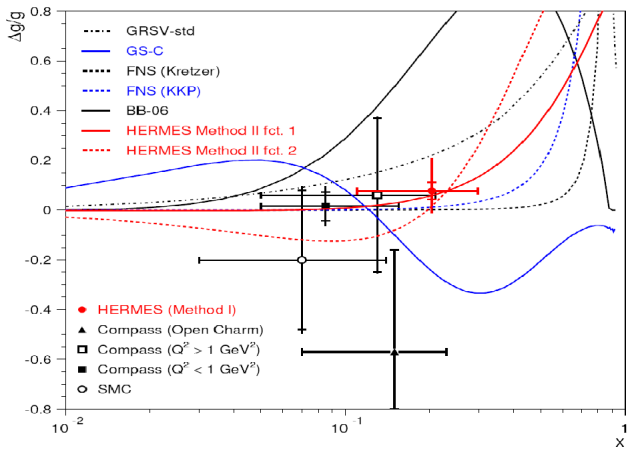

Figure 2. $\Delta g/g$ measurements [29].

• The strange quark polarization over the measured range (and within systematic uncertainties) is consistent with zero. This seems to be in contradiction with the results extracted from global analysis of inclusive data. It is important to independently verify this result.

The results of the high energy experiments left us with some open questions, such as • Is the contribution of L_q significant? • How large is the gluon contribution ΔG? • What is the flavor dependence of the spin structure?

The Jefferson Lab spin program in the last decade has helped answer some of the questions. More importantly, Jefferson Lab experiments have explored the high-x and low- to intermediate-Q^2 regions with high precision. The high-x region is where the valence quarks dominate and pQCD and quark models have predictions. The low-Q^2 region is where predictions from chiral perturbation theory, the leading effective theory of strong interaction at long distance, can be tested. Measurements in the intermediate-Q^2 region explore the transition between the descriptions of the strong force from the perturbative to nonperturbative regime of QCD. In particular, one can learn about the quark-gluon and quark-quark correlations through systematic

study of higher twist effects. It is also where one can test if the quark-hadron duality works for the spin structure functions.

3. Results from Jefferson Lab

With a high current, high polarization electron beam of energy up to 6 GeV and state-of-the-art polarized targets, Jefferson Lab has completed a number of experiments which extended the database on spin structure functions significantly, both in kinematic range (low Q^2 and high x) and in precision. The neutron results are from Hall A using polarized ^{3}He as an effective polarized neutron target and two high resolution spectrometers. The polarized luminosity reached 10^{36} s^{-1}cm^{-2} and in-beam polarization improved from 35% (1998) to over 65% (2008). The proton and deuteron results are from Hall B with the CLAS detector and Hall C with the HMS spectrometer and using polarized NH_3 and ND_3 targets with in-beam polarization of about 80% and 40% respectively.

An example of data on the proton g_1 structure function together with the world data is shown in Fig. 3. The Jefferson Lab measurements are mostly focussing on:

(i) The high-x region and the nucleon resonance region;
(ii) The moments of spin structure functions, especially at low to moderate Q^2;
(iii) The higher twist effects related to parton correlations;
(iv) The contributions to the nucleon spin puzzle.

These results will be discussed in detail in the next sections.

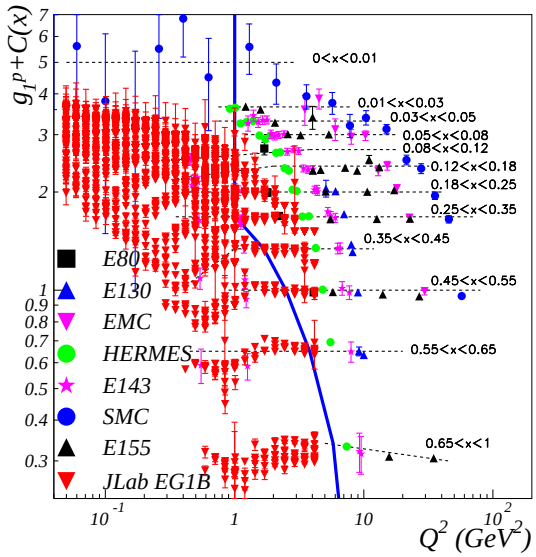

Figure 3. World results on g_1^p. The solid line is the conventional DIS frontier ($W = 2$ GeV, $Q^2 = 1$ GeV^2).

3.1. Spin structure in the valence quark (high-x) region

Jefferson Lab Hall A experiment E99-117 [32] measured the neutron asymmetry A_1^n with high precision from a polarized electron beam scattering off a ^{3}He target polarized either

longitudinally or transversely. The experiment covered an x region from 0.33 to 0.61 (Q^2 from 2.7 to 4.8 GeV^2). The results on A_1^n are shown in the left panel of Fig. 4. The experiment greatly improved the precision of data in the high-x region, providing the first evidence that A_1^n becomes positive at large x, and clearly inconsistent with SU(6) symmetry. The results are in good agreement with the LSS 2001 pQCD fit to previous world data [28] (solid curve) and the statistical model [33] (long-dashed curve). The trend of the data is consistent with the RCQM [8] predictions (the shaded band). The data disagree with the predictions from the leading order pQCD models [9] (short-dashed and dash-dotted curves).

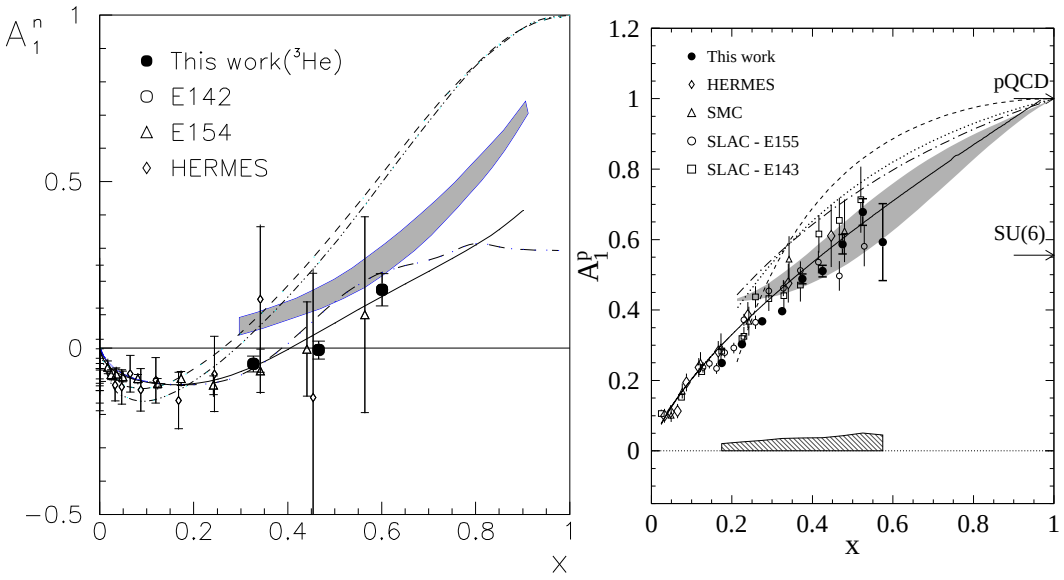

Figure 4. A_1^n (left panel) and A_1^p (right panel) results from Jefferson Lab Hall A E99-117 [32] and CLAS EG1b [34] experiments (filled circles), compared with the world data and theoretical predictions (see text for details).

New results for A_1^p and A_1^d from the Hall B EG1b experiment [34] are also available. The data cover the Q^2 range of 1.4 to 4.5 GeV^2 for x from 0.2 to 0.6 with an invariant mass larger than 2 GeV. The results on A_1^p are shown in the right panel of Fig. 4. The precision of the data improved significantly over that of the existing world data. Similar data also exist on the deuteron and once again exhibit a trend to exceed the asymmetries predicted by SU(6) (7) at large x.

In addition to the prediction by the RCQM [8] (again indicated by the shaded band), several curves based on different scenarios of SU(6) symmetry breaking in the context of quark-hadron duality, as predicted by Close and Melnitchouk [35], are also shown in the right panel of Fig. 4.

These data provide crucial input for the global fits to the world data to extract the polarized parton densities and the extractions of higher twist effects. The polarized quark distribution functions $\Delta u/u$ and $\Delta d/d$ in the high-x region were first extracted, in the leading order approximation, from the Hall A neutron data and the world proton data (left panel of Fig. 5) [32]. A recent leading order extraction used also the CLAS EG1b proton and deuteron data and the world data. The results are shown in the right panel of Fig. 5, along with predictions from leading order pQCD [9] (dashed curves) and a pQCD fit (solid line) including quark orbital angular momentum contributions [11]. The results for $\Delta d/d$ are in significant disagreement with the predictions from the leading order pQCD model assuming hadron helicity conservation. The data agree better with the fit including quark orbital angular momentum, suggesting that

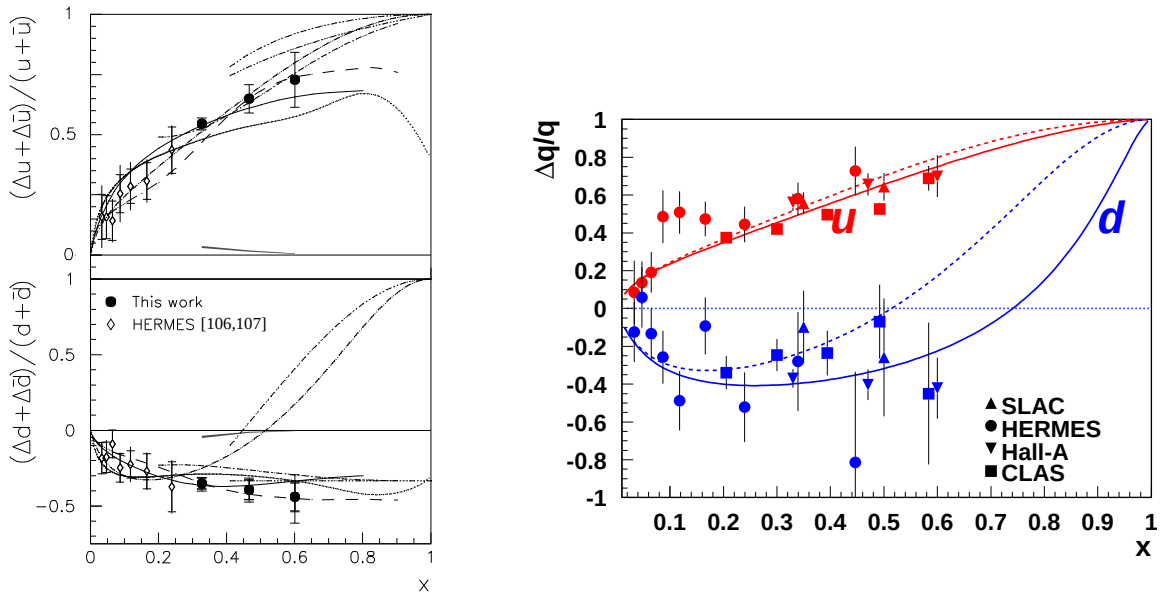

Figure 5. $\Delta u/u$ (upper side of both panels) and $\Delta d/d$ (lower side of both panels) results from Jefferson Lab Hall A E99-117 [32] together with world data (left panel) and CLAS EG1b [34] experiments (right panel), compared with the world data and theoretical predictions (see text for details).

it may play an important role in this kinematic region. However the pQCD fit still predicts that $\Delta d/d \to 1$ when x approaches 1, in contrast to the predictions from the relativistic valence quark models [8] and diquark models [36] that it stays negative.

3.2. Moments of spin structure functions

The spin structure functions g_1 and g_2 (or σ_{TT} and σ_{LT}) were measured in Hall A experiment E94-010 on ^{3}He from breakup threshold to $W = 2$ GeV covering the Q^2 range of 0.10-0.9 GeV^2. The extended GDH integrals $I(Q^2) = \int_{thr.}^{\infty} \sigma_{TT}(\nu, Q^2) d\nu/\nu$ (open symbols) were extracted for ^{3}He [37] (right panel of Fig. 6) and for the neutron [38] (left panel). The solid squares include an estimate of the unmeasured high energy part.

The ^{3}He results rise with decreasing Q^2. Since the GDH sum rule at $Q^2 = 0$ predicts a large negative value, a drastic turn around should happen at Q^2 lower than 0.1 GeV^2. A simple model using MAID plus quasi-elastic contributions estimated from a PWIA model [42] indeed shows the expected turn around. The data at low Q^2 should be a good testing ground for few-body chiral perturbation theory calculations.

The neutron results indicate a drastic yet smooth variation of $I(Q^2)$ to increasingly negative values as Q^2 varies from 0.9 GeV^2 towards zero. The data are more negative than the MAID model calculation [40]. Since the calculation only includes contributions to $I(Q^2)$ for $W \leq 2$ GeV, it should be compared with the open squares. The GDH sum rule prediction, $I(0) = -232.8\,\mu$b, is indicated along with extensions to $Q^2 > 0$ using two NLO χPT calculations, one using the heavy baryon approximation (HBχPT) [39] (dotted line) and the other relativistic baryon χPT (RBχPT) [20] (dot-dashed line). Shown with a band is RBχPT including resonance effects [20], which have an associated large uncertainty due to the resonance parameters used.

The first moment of g_1, Γ_1, was extracted from E94-010 [38] for the neutron and ^{3}He [37]. CLAS experiment EG1 [34] measured g_1 for the proton and the deuteron covering the resonance

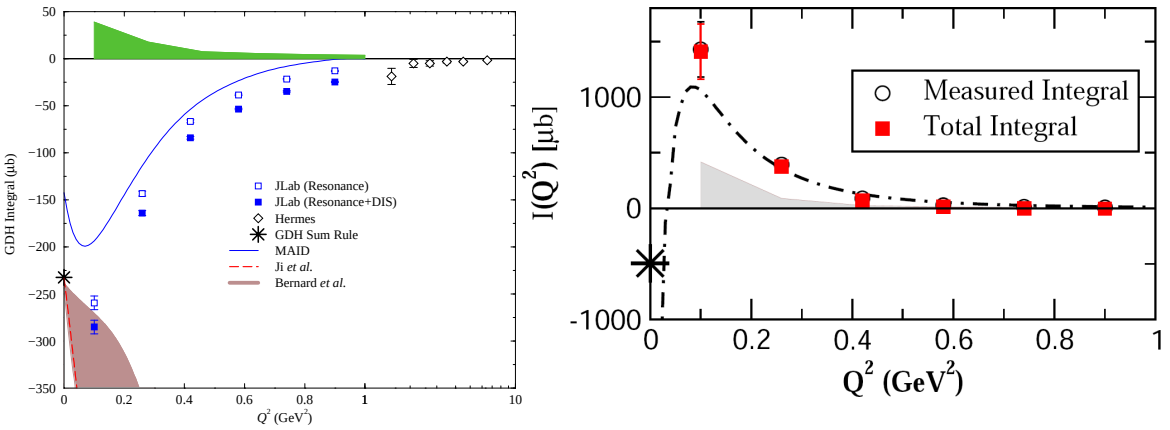

Figure 6. Results of GDH sum $I(Q^2)$ for neutron (left) and ^{3}He (right). The ^{3}He GDH results are compared with the MAID model plus a quasi-elastic contribution. The neutron GDH results are compared with χPT calculations of Ref. [39] (dashed line) and Ref. [20] (shaded band). The MAID model calculation of Ref. [40], is represented by the solid line. Data from HERMES [41] are also shown.

region and beyond over a Q^2 range from 0.05 to 5 GeV^2. The first moments were extracted for the proton, the deuteron and the neutron (from the deuteron with the proton contribution subtracted). The results are plotted in Fig. 7. Also plotted is the first moment for $p-n$ [43], a flavor non-singlet combination, which is the Bjorken sum at large Q^2 (13). These moments show a strong yet smooth variation in the transition region (Q^2 from 1 to 0.1 GeV^2). The Bjorken sum was used to extract the strong coupling constant α_s at high Q^2 (5 GeV^2). An attempt was made to extract an effective coupling α_{s,g_1} at low Q^2 region using the Bjorken sum, see Sec. 3.6.

At large Q^2 the data agree with pQCD models with little higher twist effects. At low Q^2 two calculations using chiral perturbation theory are compared with the Γ_1 data and are in reasonable agreement at the lowest Q^2 value (0.05–0.1 GeV^2).

The x^2 (or equivalently, additional $1/\nu^2$) weighted moments at low Q^2 are related to the generalized spin polarizabilities γ_0 (15) and δ_{LT} (16). They were expected to provide a more reliable test of χPT at low Q^2 because the unmeasured contributions from the high energy (low-x) region are strongly suppressed. In particular, δ_{LT} provides a benchmark test of χPT since the $\Delta(1232)$ contribution, which is difficult to treat in χPT, is suppressed. Figure 8 presents results of the generalized spin polarizabilities γ_0 and δ_{LT} for the neutron [38], and γ_0 for the proton [34] and for the isospin decompositions $p-n$ and $p+n$ [43]. There are strong disagreements between data and χPT calculations. In particular, the disagreement in δ_{LT}^n with both χPT predictions presents a significant challenge to present formulations of chiral perturbation theory. Experimental results at very low Q^2 (down to 0.02 GeV^2) for both the neutron [46] and the proton [47] should be available soon. Further theoretical and experimental efforts will be needed to clarify the situation. In particular, a planned measurement of δ_{LT} for the proton [48] should shed light on this "puzzle".

Lattice QCD results for the transition region are not yet available. An important aspect of the lattice calculation is the extrapolation to the physical mass of the pion. This extrapolation is guided by χPT calculations. Since these calculations have strong disagreements with some of the observables discussed here, one could question the reliability of the chiral extrapolation.

Finally, another important result on the experimental level is the good agreement between the neutron information extracted from a deuteron and a ^{3}He target. It validates the use of

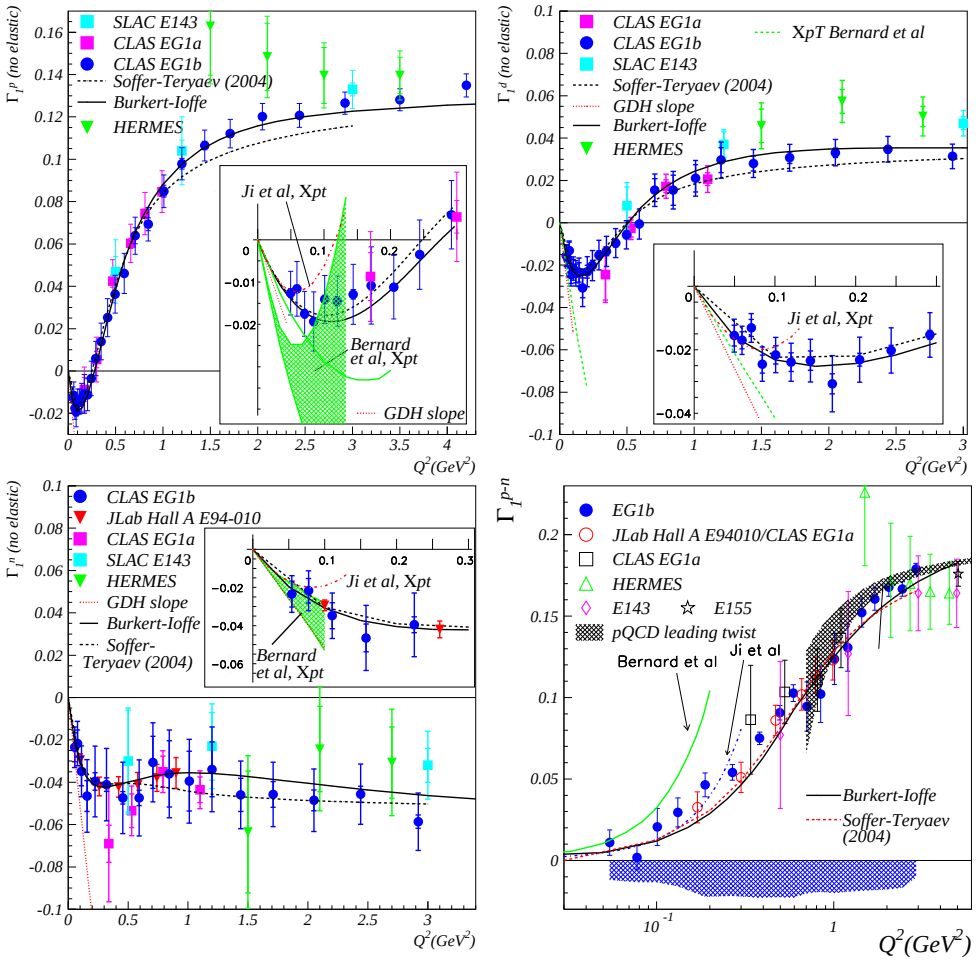

Figure 7. Results of $\Gamma_1(Q^2)$ for p, d, n and $p-n$ from Jefferson Lab Hall A and CLAS EG1. The slopes at $Q^2 = 0$ predicted by the GDH sum rule are given by the dotted lines. The dashed (solid) lines are the predictions from the Soffer-Teryaev [44] (Burkert-Ioffe [45]) model. The leading twist Q^2 evolution of the moments is given by the gray band. The insets show comparisons with χPT calculations by Ji *et al.* [39] and Bernard *et al.* [20].

polarized deuteron and ^{3}He, at least within the precision of the Jefferson Lab data.

3.3. Measurements of g_2, moments of g_2 and higher twist effects

The measurements of g_2 require tranversely polarized targets. SLAC E155x [49] performed the only dedicated g_2 measurement prior to Jefferson Lab. At Jefferson Lab, g_2 and its moments have been extensively measured for the neutron with a polarized ^{3}He target in a wide range of kinematics in several Hall A experiments (E94-010 [38], E97-103 [50], E99-117 [32], E02-012 [51] and E97-110 [46]). The measurement on the proton was performed in the RSS experiment in Hall C at an average Q^2 of 1.3 GeV^2.

Figure 9 shows the world data on g_2^n in the DIS ($W > 2$ GeV) region. The precision data from E97-103 show for the first time a clear deviation from g_2^{WW}, indicating that twist-3 (or higher) effects are important at Q^2 around 1 GeV^2 and lower.

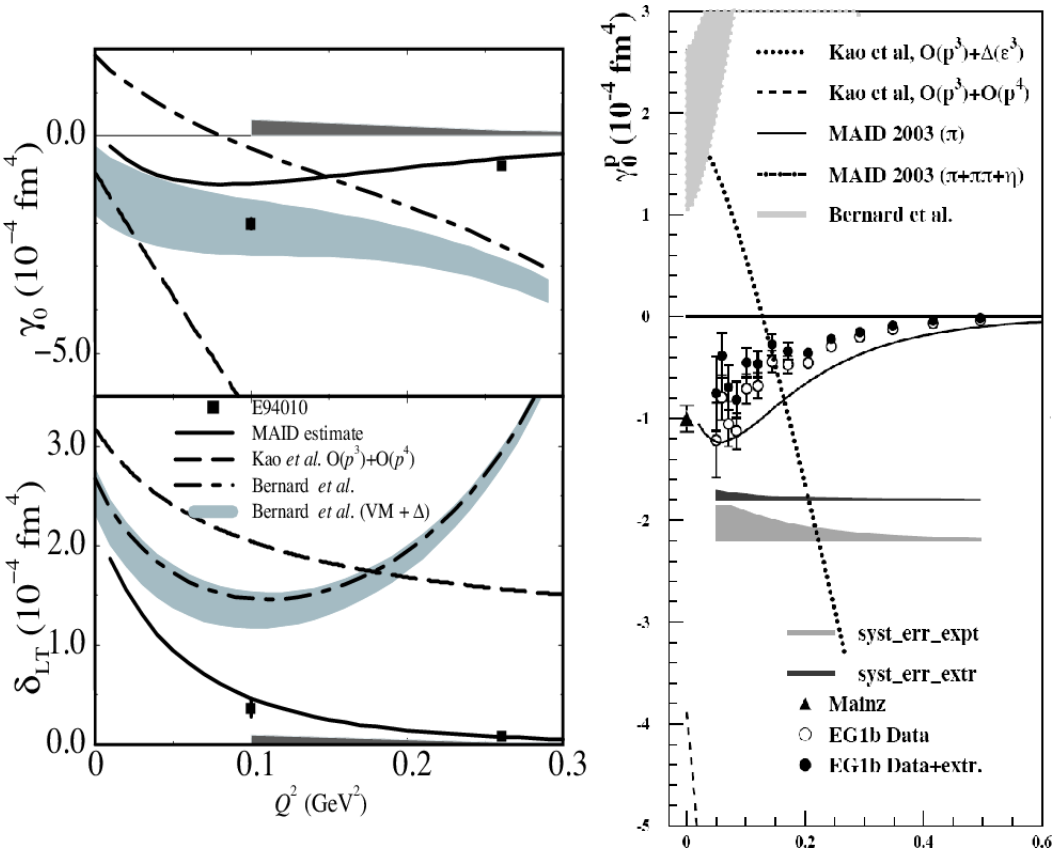

Figure 8. Generalized spin polarizabilities. The neutron generalized forward spin polarizabilities γ_0^n and δ_{LT}^n (left plots) were extracted from the Hall A E94-010 data. γ_0^p (right plot) was extracted from the CLAS EG1 data.

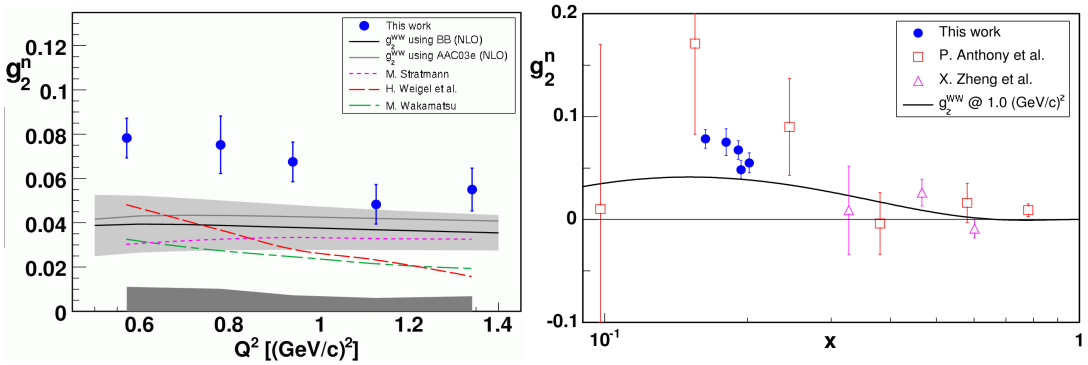

Figure 9. Results from experiment E97-103 on g_2^n. (Left) g_2^n vs Q^2 from E97-103, models and the twist-2 term g_2^{WW}. (Right) g_2^n *vs.* x from experiments E97-103, E99-117 and SLAC E155x. All data are at $W > 2$ GeV.

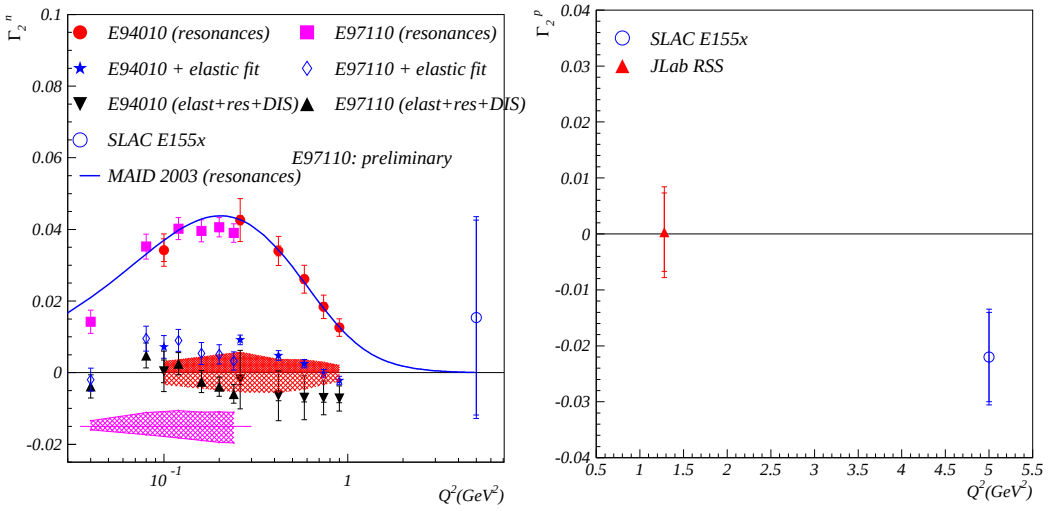

Figure 10. The verification of the BC sum rule from Hall A experiments E94-010 and E97-110 (neutron, left) and Hall C RSS (proton, right), together with SLAC E155x data.

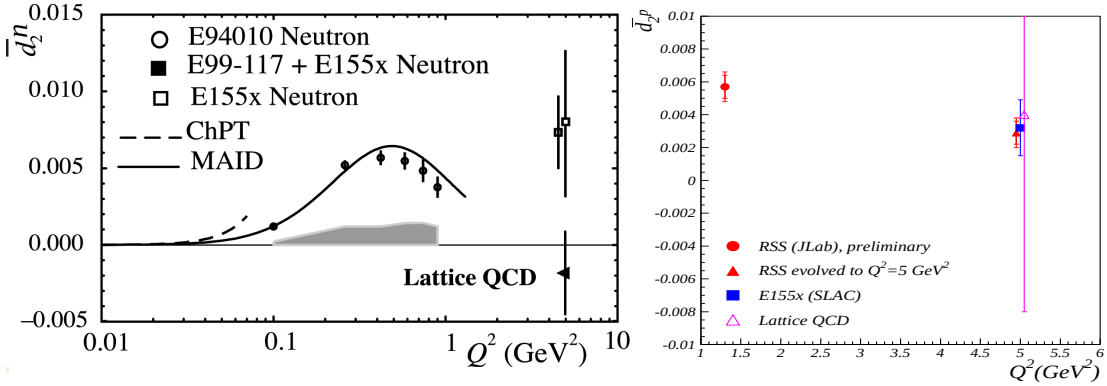

Figure 11. The x^2-weighted moment d_2 of the neutron (left) and proton (right).

The first moment of g_2 is expected to be zero at all Q^2 from the Burkhardt-Cottingham sum rule. The measurements for the proton and the neutron are shown in Fig. 10. The precision data are consistent with the BC sum rule in all cases, indicating that g_2 is a well behaved function (with good convergence at high energy).

The second moment of $g_2 - g_2^{WW}$ has also been formed from E94-010 (neutron) and RSS (proton and neutron), see Fig. 11. The E94-010 results were compared to a chiral perturbation theory calculation [39] and the MAID parametrization [40]. Furthermore, the Hall A experiment E99-117 provided data on g_2^n at high x, see right plot on Fig. 9. Combining these results with the SLAC data, the second moment d_2^n was extracted at an average Q^2 of 5 GeV^2 with much improved uncertainty. While a negative or near-zero value was predicted by lattice QCD and most models, the result for d_2^n at an average Q^2 of 5 GeV^2 is positive.

The high precision data allowed new analyzes [43, 52] to study higher twist contributions from the g_1 moments. In particular, the twist-4 matrix element f_2 was extracted by fitting Γ_1 up to $\mathcal{O}(1/Q^6)$. The same analysis was also performed on the Bjorken sum.

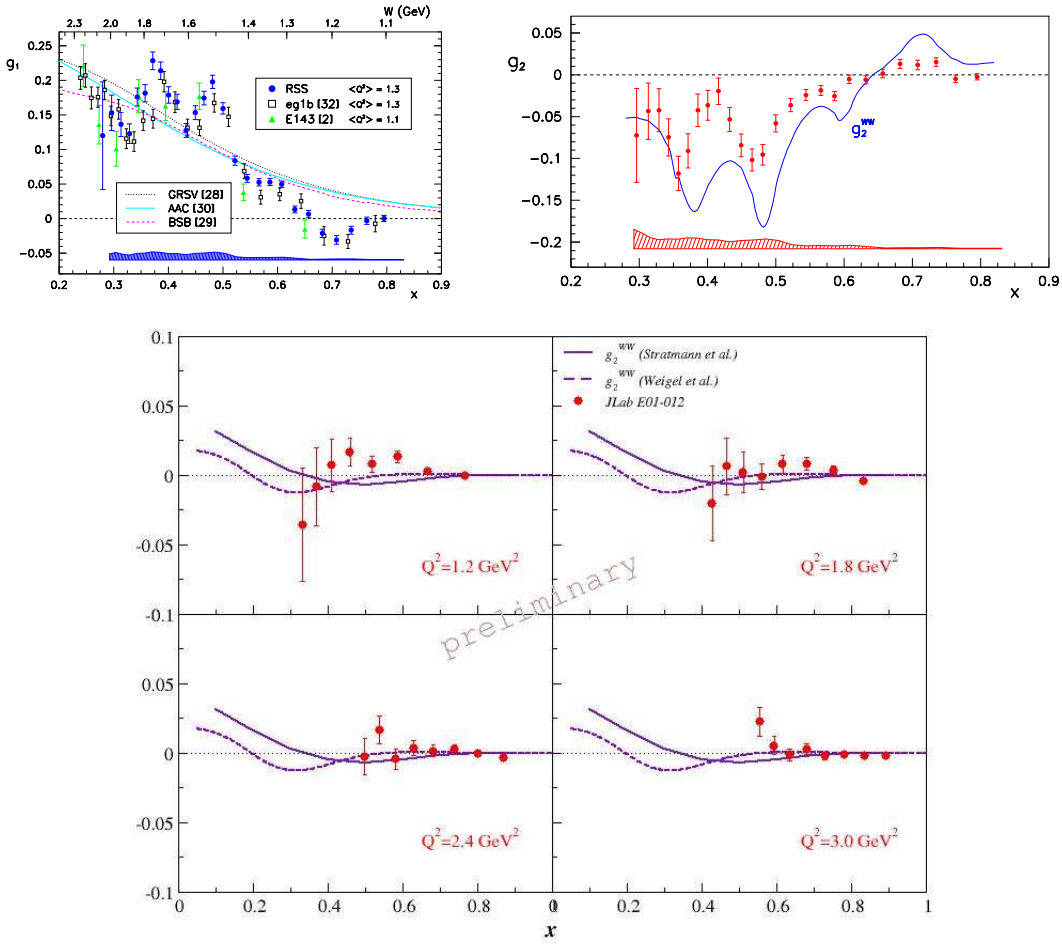

Figure 12. Results from the RSS experiment for g_1 (top-left panel) and g_2 (top-right panel) for the proton in the resonance region measured at $\langle Q^2 \rangle = 1.3$ GeV^2, and results from the Hall A experiment E01-012 (bottom panel) for g_2^n in the resonance region measured at $Q^2 = 1.2 - 3$ GeV^2.

With the high precision data at low Q^2 and high x, the higher twist contributions were included in the new global polarized PDF analysis [28] for the first time. The dynamical twist effects are important at moderate x but become smaller at low and high x. At large x, however, g_1 being small, the relative contributions of the higher twist effects are still significant. At $Q^2 < 1$ GeV^2, the overall effects of higher twists become non-negligible.

3.4. Quark-hadron duality in spin structure functions

A detailed study of duality in the spin structure functions g_1^p and g_1^d has been published by the EG1 collaboration [34]. As shown in Fig. 13, one observes a clear trend of strong, resonant deviations from the scaling curve at lower Q^2, towards a pretty good agreement at intermediate Q^2. The integral of g_1 over the whole resonance region begins to agree with the NLO results above $Q^2 \approx 1.7$ GeV^2. The results on the proton and deuteron from EG1b [34] thus indicate a much slower approach to "global" duality for the polarized structure function g_1 than has been observed for unpolarized structure functions. Local duality seems violated in the Δ resonance region even for Q^2 values as high as 5 GeV^2. The data taken by the RSS collaboration in

Hall C [53] (see Fig. 12) corroborate these observations and add more precise data points for $Q^2 \approx 1.3$ GeV^2.

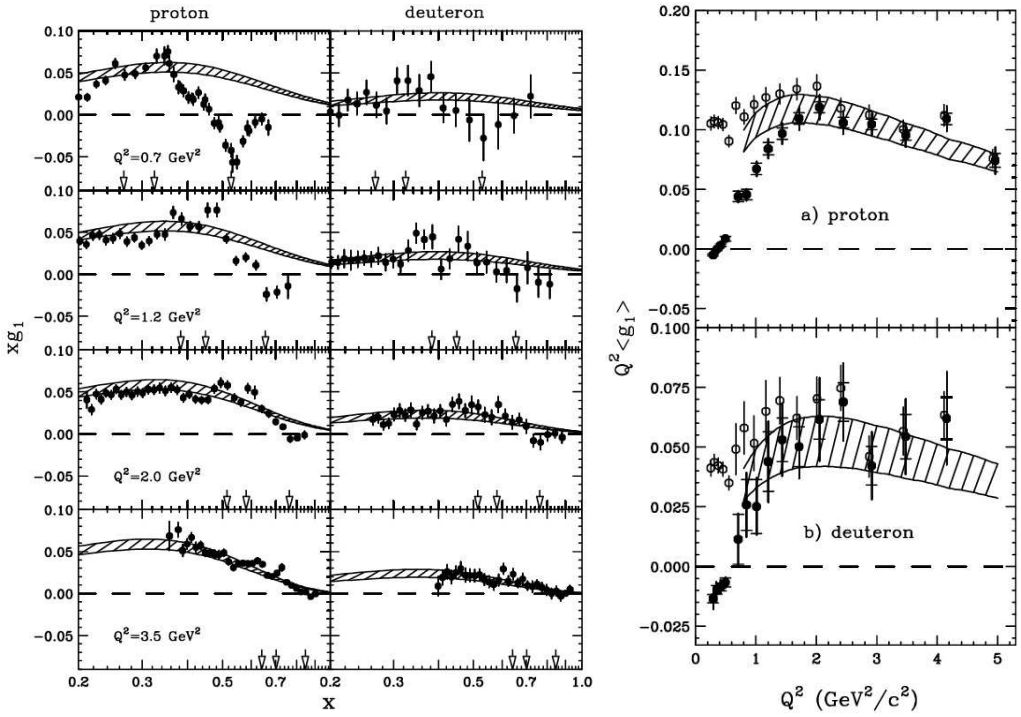

Figure 13. Data on g_1 of the proton and the deuteron from Jefferson Lab Hall B (left panel) and its average over the resonance region (right panel). Prominent resonances are indicated by arrows in the left panel. The hashed curves represent the range of extrapolated DIS results from modern NLO fits (GRSV and AAC), evolved to the Q^2 of the data and corrected for target mass effects. The open circles in the right panel include the elastic contribution, while the filled circles are only integrated over $W > 1.08$ GeV.

The spin structure functions g_1 and A_1 were measured in the resonance region ($W < 2$ GeV) in the Hall A ^{3}He experiments E94010 [38] (in the Q^2 region below 1 GeV^2) and E01012 [51] (from 1 GeV^2 to 4 GeV^2). The results for $A_1^{^3\mathrm{He}}$ above 1 GeV^2 are presented in Fig. 14 (left panel). Also plotted are the world DIS data and a fit to the DIS data. Due to the prominent contributions from the Δ resonance, local duality does not appear to work at low Q^2 (below 2 GeV^2). At high Q^2 (above 2 GeV^2), the Δ resonance contribution starts to diminish. It is interesting to note that the two sets of resonance data at the highest Q^2 (2.9 and 4 GeV^2) agree well, indicating little or no Q^2 dependence, which is a key feature of the DIS data. These data also show the trend of becoming positive at the high-x side, the same trend as observed for DIS data. The resonance data were integrated to study global duality. Figure 14 (right panel) shows the results for both ^{3}He and the neutron in comparison with the DIS fits evolved to the same Q^2. The resonance data agree with the DIS fits at least for Q^2 higher than 1.8 GeV^2, indicating that global duality holds for the neutron and ^{3}He g_1 spin structure function in the high Q^2 region (above 1.8 GeV^2).

The study of quark-hadron duality helps us to study higher twist effects and to extend the kinematic region where one might be able to apply partonic interpretations. From a practical point of view, the good understanding of the higher twist effects and quark-hadron duality allows us to considerably extend the experimental database used to extract the polarized parton

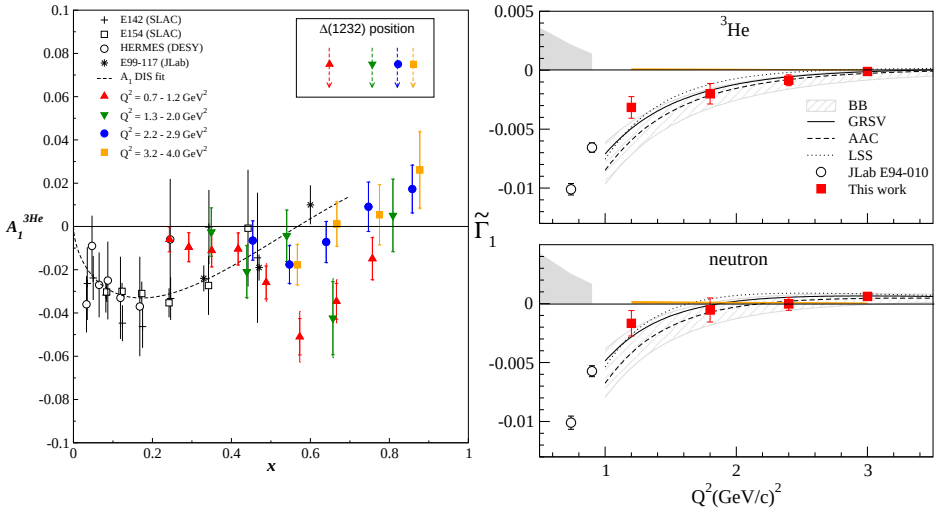

Figure 14. $A_1^{^3\mathrm{He}}$ (left panel) in the resonance region from Jefferson Lab E01-012, compared with the world DIS data and a fit. $\Gamma_1^{^3\mathrm{He}}$ and Γ_1^n (right panel) of the resonance region from Jefferson Lab E01-012, together with lower Q^2 results from Jefferson Lab E94-010, compared with the world DIS fits.

distributions [28], see Fig. 3.

3.5. The constraint on ΔG

The doubly polarized inclusive data from Jefferson Lab yield information on the spin of the nucleon carried by gluons, ΔG. The LSS group [28] included the Jefferson Lab data from Hall A (experiment E99-117) and CLAS experiment EG1 in their global analysis. The central values of the polarized parton distributions (Fig. 1) did not change significantly, but their uncertainties were noticeably reduced, see Fig. 15. In particular, the uncertainty on Δg is significantly reduced: by a factor 2 near $x = 0.3$ and 4 near $x = 0.5$ (within the model assumed for Δg by the LSS group).

3.6. The effective strong coupling at large distance

In QCD, the magnitude of the strong force is given by the running coupling constant α_s. At large Q^2, in the pQCD domain, α_s is well-defined and can be experimentally extracted, *e.g.* using the Bjorken sum rule (13). The pQCD definition leads to an infinite coupling at large distances, when Q^2 approaches Λ^2_{QCD}. This is not a conceptual problem because here one is outside the validity domain of pQCD. Since the data show no sign of discontinuity when crossing the intermediate Q^2 domain, see *e.g.* Fig. 7, it is natural to look for a definition of an effective coupling α_s^{eff} which works at any Q^2, and matches α_s at large Q^2 but stays finite at small Q^2. The Bjorken sum rule can be used advantageously to define α_s^{eff} at low Q^2 [54]. The data on the Bjorken sum are used to experimentally extract α_s^{eff} following a prescription by Grunberg [55], see Fig. 16. The Bjorken and GDH sum rules also allow us to determine α_s^{eff} at respectively large Q^2 and $Q^2 \simeq 0$. The extracted α_s^{eff} provides for the first time an effective coupling at all Q^2, albeit one that is process dependent. An interesting feature is that α_s^{eff} becomes scale invariant at small Q^2, which was predicted by a number of calculations.

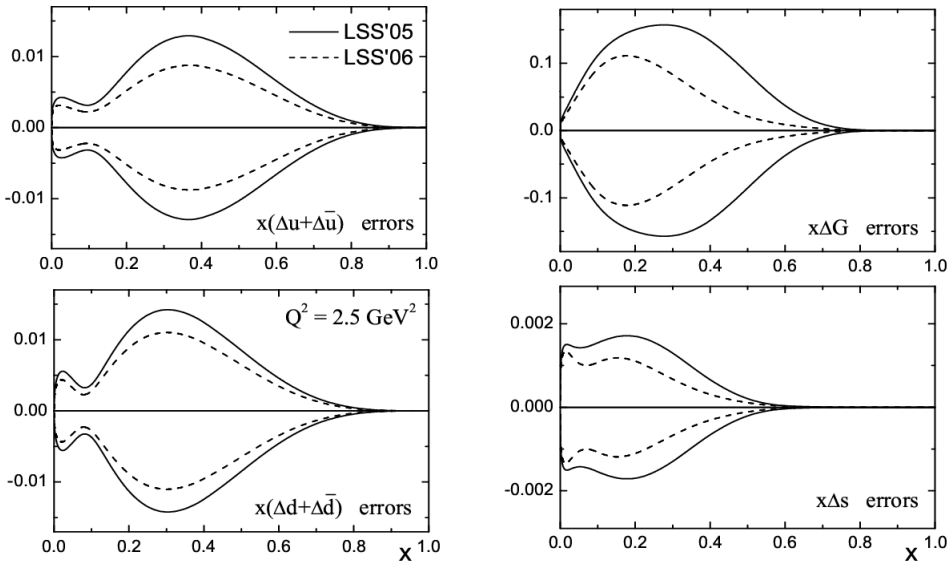

Figure 15. Uncertainty on the polarized parton distributions. Solid curves do not include Jefferson Lab data, and uncertainties are reduced after including the Hall A E99-117 and Hall B EG1 data (dashed curves).

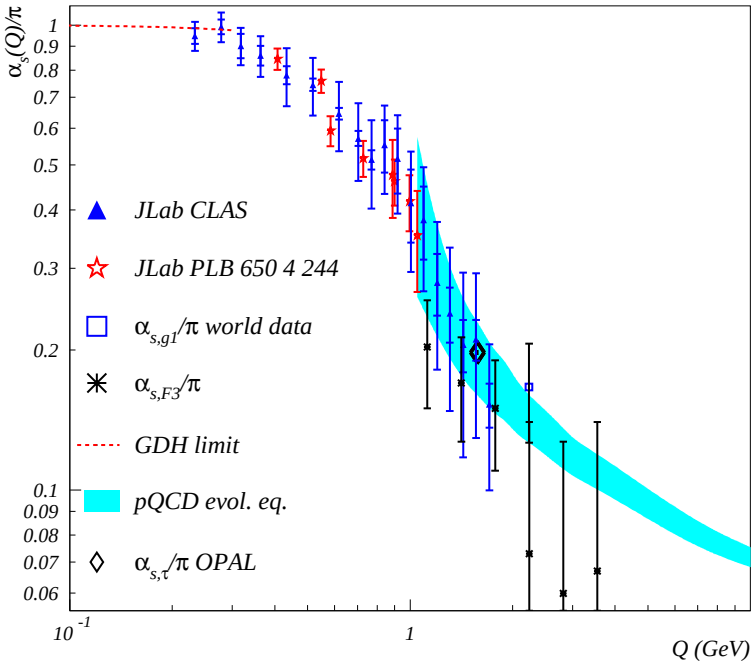

Figure 16. Value of α_s^{eff}/π extracted from the data on the Bjorken sum, on τ decay, and on the Gross-Llewellyn Smith sum rule. The values of α_s^{eff} computed within pQCD and using the Bjorken sum is given by the shaded band. The values of α_s^{eff}/π extracted using the GDH sum rule is given by the dashed line.

4. Transverse spin structure

To fully understand the nucleon structure, the transverse dimension can no longer be neglected. In the last few years, there has been a surge of interest in the nuclear physics community in the transverse spin and transverse momentum dependent distributions [56]. First experimental results of single target spin asymmetries in semi-inclusive DIS from HERMES [26] (for the proton) and COMPASS [27] (for the deuteron and the proton) showed clear nonzero results for both the Collins [57] and Sivers [58] asymmetries. These initial explorations demonstrated the importance of the transverse spin (transversity) and the quark orbital angular momentum.

A recently completed Jefferson Lab experiment [59] is the first one to measure the single-spin asymmetry on the neutron with a transversely polarized ^{3}He target. The goal of this experiment is to provide the first measurement of the neutron transversity and Sivers function, complementary to the HERMES and COMPASS measurements on the proton and deuteron. This experiment focuses on the valence quark region, $x = 0.19 - 0.34$, at $Q^2 = 1.77 - 2.73$ GeV^2. Data from this experiment, when combined with data from HERMES [26], COMPASS [27] and Belle [60], will provide powerful constraints on the transversity distributions of both u-quarks and d-quarks in the valence region. Due to the good particle identification in the HRS, kaon data were collected at the same time, providing a set of data to study the transverse spin asymmetries for semi-inclusive $K^{\pm}$ production.

In Hall B, study of the transverse momentum dependent distributions is one of the main goals of an ongoing experiment [61] with a polarized beam on a longitudinally polarized proton target. Future measurements are planned with tranversely polarized proton and deuteron targets [62].

5. Conclusions and perspective

In summary, the high polarized luminosity available at Jefferson Lab has provided us with high precision data to study the nucleon spin structure in a wide kinematic range. They shed light on the valence quark structure, help to understand quark-gluon correlations, allow us to study the nonperturbative region and to explore the transition between perturbative and nonperturbative regions of QCD. A planned precision study on transverse spin phenomena will open a new window to study the nucleon structure and help us understand the strong interaction.

The 12 GeV energy upgrade [63] opens up a much wider DIS kinematics region to study nucleon spin structure. Planned experiments [64] in the high-x region will definitively establish the contributions of valence quarks to the nucleon structure. A precision measurement of the moment d_2 [65] will provide a benchmark test of lattice QCD predictions. An extensive semi-inclusive DIS program [66] with transversely and longitudinally polarized neutron and proton targets will map out precisely the Collins and Sivers moments and other transverse momentum dependent observables. The tensor charge, a fundamental quantity of the nucleon, will be determined, which will provide another benchmark test of lattice QCD predictions. The 6 and 12 GeV data, together, will complete our picture of nucleon spin structure in the valence region.

A new facility, an electron-ion collider (EIC), is undergoing discussion in the US hadronic-physics community [67], as a long-term future facility. It will provide unique capabilities for the study of QCD well beyond all existing facilities. It will extend the spin structure study over a very wide region.

Acknowledgments

The work is supported by the US Department of Energy (DOE). Jefferson Science Associates operates the Thomas Jefferson National Accelerator Facility for the DOE under contract DE-AC05-84ER-40150.

References

[1] S. E. Kuhn, J. P. Chen and E. Leader, Prog. Part. Nucl. Phys. **63**, 1 (2009).
[2] S. Wandzura and F. Wilczek, Phys. Lett. B **72** (1977).
[3] X. Ji and W. Melnitchouk, Phys. Rev. D **56**, 1 (1997).
[4] M. Göckeler, *et al.*, Phys. Rev. D **63**, 074506 (2001).
[5] M. Stratmann, Z. Phys. C **60**, 763 (1993).
[6] H. Weigel, Pramana **61**, 921 (2003).
[7] M. Wakamatsu, Phys. Lett. B **487**, 118 (2000).
[8] N. Isgur, Phys. Rev. D **59**, 034013 (1999); F. E. Close and A. Thomas, Phys. Lett. B **212**, 227 (1988).
[9] G. R. Farrar and D. R. Jackson, Phys. Rev. Lett. **35**, 1416 (1975); S. Brodsky, M. Burkardt and I. Schmidt, Nucl. Phys. **B441**, 197 (1995).
[10] F. Close, Nucl. Phys. **B80**, 269 (1974).
[11] H. Avakian, S. Brodsky, A. Deur and Y. Feng, Phys. Rev. Lett. **99**, 082001 (2007).
[12] J. P. Chen, A. Deur and Z. E. Meziani, Mod. Phys. Lett. A **20**, 2745 (2005).
[13] D. Drechsel, B. Pasquini and M. Vanderhaeghen, Phys. Rep. **378**, 99 (2003); D. Drechsel and L. Tiator, Ann. Rev. Nucl. Part. Sci. **54**, 69 (2004).
[14] J. Ellis and R. L. Jaffe, Phys. Rev. D **9**, 1444 (1974); *ibid.*, D **10**, 1669 (1974).
[15] H. Burkhardt and W. N. Cottingham, Ann. Phys. (N.Y.) **56**, 453 (1970).
[16] J. D. Bjorken, Phys. Rev. **148**, 1467 (1966).
[17] S. B. Gerasimov, Sov. J. Nucl. Phys. **2**, 598 (1965); S. D. Drell and A. C. Hearn, Phys. Rev. Lett. **162**, 1520 (1966).
[18] X. Ji and J. Osborne, J. Phys. G **27**, 127 (2001).
[19] C. W. Kao, T. Spitzenberg and M. Vanderhaeghen, Phys. Rev. D **67**, 016001 (2003).
[20] V. Bernard, T. Hemmert and U.-G. Meissner, Phys. Rev. D **67**, 076008 (2003).
[21] E. D. Bloom and F. J. Gilman, Phys. Rev. Lett. **25**, 1140 (1970).
[22] A. De Rujula, H. Georgi and H. D. Politzer, Phys. Lett. B **64**, 428 (1976).
[23] W. Melnitchouk, R. Ent and C. Keppel, Phys. Rep. **406**, 127 (2005).
[24] C. Bourrely, J. Soffer and O. V. Teryaev, Phys. Lett. B **420**, 375 (1998).
[25] J. Soffer, Phys. Rev. Lett. **74**, 1292 (1995).
[26] A. Airapetian, *et al.*, Phys. Rev. Lett. **94**, 012002 (2005).
[27] V. Y. Alexakhin *et al.*, Phys. Rev. Lett. **94**, 202002 (2005); E. S. Ageev *et al.*, Nucl. Phys. **B765**, 31 (2007).
[28] E. Leader, A. V. Sidorov and D. B. Stamenov, Eur. Phys. J. C **23**, 479 (2002); Phys. Rev. D **73**, 034023 (2006); Phys. Rev. D **75**, 074027 (2007).
[29] See *e.g.* N. Bianchi, in talk presented at Pacific-SPIN07, www.triumf.info/hosted/pacspin07/talks/Bianchi.ppt.
[30] B. W. Filippone and X. Ji, Adv. Nucl. Phys. **26**, 1 (2001)
[31] F. Myhrer and A. W. Thomas, Phys. Lett. B **663**, 302 (2008)
[32] X. Zheng *et al.*, Phys. Rev. Lett. **92**, 012004 (2004); Phys. Rev. C **70**, 065207 (2004).
[33] C. Bourrely, J. Soffer and F. Buccella, Eur. Phys. J. C **23**, 487 (2002).
[34] R. Fatemi *et al.*, Phys. Rev. Lett. **91**, 222002 (2003); J. Yun *et al.*, Phys. Rev. C **67**, 055204 (2003); K. V. Dharmawardane *et al.*, Phys. Lett. B **641** 11 (2006); Y. Prok *et al.*, Phys. Lett. B **672**, 12 (2009); P. Bosted *et al.*, Phys. Rev. C **75**, 035203 (2007).
[35] F. E. Close and W. Melnitchouk, Phys. Rev. C **68**, 035210 (2003).
[36] I. C. Cloet, W. Bentz and A. W. Thomas, Phys. Lett. B **621**, 246 (2005).
[37] K. J. Slifer *et al.*, Phys. Rev. Lett **101**, 022303 (2008).
[38] M. Amarian *et al.*, Phys. Rev. Lett. **89**, 242301 (2002); Phys. Rev. Lett. **92**, 022301 (2004).
[39] X. Ji, C. Kao and J. Osborne, Phys. Lett. B **472**, 1 (2000).
[40] D. Drechsel, S. Kamalov and L. Tiator, Phys. Rev. D **63**, 114010 (2001)
[41] A. Airapetian *et al.*, Phys. Rev. Lett. **90**, 092002 (2003); Eur. Phys. J. C **26**, 527 (2003); Phys. Rev. D **75**, 012007 (2007).
[42] C. Ciofi degli Atti, E. Pace and G. Salme, Phys. Rev. C **51**, 1108 (1995).
[43] A. Deur *et al.*, Phys. Rev. Lett. **93**, 212002 (2004); Phys. Rev. D **78**, 032001 (2008).
[44] J. Soffer and O. V. Teryaev, Phys. Rev. D **70**, 116004 (2004).
[45] V. D. Burkert and B. L. Ioffe, Phys. Lett. B **296**, 223 (1992).
[46] Jefferson Lab Experiment E97-110, J. P. Chen, A. Deur and F. Garibaldi, spokespersons.
[47] Jefferson Lab Experiment E03-006, M. Battaglieri, A. Deur, R. De Vita and M. Ripani, spokespersons.
[48] Jefferson Lab Experiment E08-027, A. Camsonne, J. P. Chen and K. Slifer, spokespersons.
[49] P. L. Anthony *et al.*, Phys. Lett. B **553**, 18 (2003).
[50] K. Kramer *et al.*, Phys. Rev. Lett. **95**, 142002 (2005).
[51] P. Solvignon *et al.*, Phys. Rev. Lett. **101**, 182502 (2008).

[52] Z. E. Meziani *et al.*, Phys. Lett. B **613**, 148 (2005); M. Osipenko *et al.*, Phys. Lett. B **609**, 259-264 (2005).
[53] F. R. Wesselmann *et al.*, Phys. Rev. Lett. **98**, 132003 (2007).
[54] A. Deur, V. Burkert, J. P. Chen and W. Korsch, Phys. Lett. B **650**, 244 (2007); Phys. Lett. B **665**, 349 (2008).
[55] G. Grunberg, Phys. Lett. B **95**, 70 (1980); Phys. Rev. D **29**, 2315 (1984); Phys. Rev. D **40**, 680 (1989).
[56] P. Mulders and R. D. Tangerman, Nucl. Phys. **B461**, 197 (1996).
[57] J. Collins, Nucl. Phys. **B396**, 161 (1993).
[58] D. W. Sivers, Phys. Rev. D **41**, 83 (1990).
[59] Jefferson Lab Experiment E06-010, J. P. Chen, E. Cisbani, H. Gao, X. Jiang and J.-C. Peng, spokespersons.
[60] A. Ogawa *et al.*, AIP Conf. Proc. **792**, 949 (2005).
[61] Jefferson Lab Experiment E05-113, H. Avakian, P. Bosted, D. Crabb and K. Griffioen, spokespersons.
[62] Jefferson Lab Experiment E08-015, H. Avakian, P. Bosted, K. Hafidi, N. Makins and P. Rossi, spokespersons.
[63] Conceptual Design Report for the Science and Experimental Equipment for the 12 GeV Upgrade of CEBAF (2005).
[64] Jefferson Lab Experiment E12-06-110, G. Cates, J. P. Chen, Z. E. Meziani and X. Zheng, spokespersons; Jefferson Lab E12-06-109, S. Kuhn *et al.*, spokespersons.
[65] Jefferson Lab Experiment E12-06-121, T. Averett, W. Korsch, Z. E. Meziani and B. Sawatzky, spokespersons.
[66] A. Afanasev *et al.*, hep-ph/0703288; Jefferson Lab Experiment PR09-014, J. P. Chen, H. Gao, X. Jiang, J. C. Peng and X. Qian, spokespersons; Jefferson Lab Experiment E12-07-107, H. Avakian *et al.*, spokespersons; Jefferson Lab Experiment E12-09-009, H. Avakian *et al.*, spokespersons.
[67] The Nuclear Science Advisory Committee Report: "The Frontiers of Nuclear Science - A Long Range Plan" (2007).